

Research Article



Coordination Chemistry

How to cite: *Angew. Chem. Int. Ed.* **2025**, *64*, e202509199 doi.org/10.1002/anie.202509199

Tailoring the Magnetic Properties of 2D Metal-Organic Networks by Harnessing the Coordination Sphere

Shanmugasibi K. Mathialagan⁺, Sofia O. Parreiras⁺,* José Santos⁺, Cristina Martín-Fuentes, Daniel Moreno, Lenka Černa, Maria Tenorio, Beatriz Muñiz-Cano, Koen Lauwaet, Manuel Valvidares, Miguel A. Valbuena, José I. Urgel, Wolfgang Kuch, Pierluigi Gargiani, Rodolfo Miranda, José I. Martínez,* José M. Gallego, Nazario Martín,* and David Écija*

Abstract: Achieving magnetic ordering in low-dimensional materials remains a key objective in the field of magnetism. Herein, coordination chemistry emerges as a powerful discipline to promote the stabilization of magnetism at the nanoscale. We present a thorough study of exemplary two-dimensional metal-organic nanoarchitectures synthesized on a Au(111) substrate, which are rationalized by using surface-science techniques and theoretical calculations. By tuning the stoichiometry, two distinct phases based on the same molecular linker coordinated with Co atoms are obtained, though featuring a different coordination sphere. Remarkably, our combined experimental and theoretical results suggest that for one phase the Co centers have an out-of-plane antiferromagnetic ground state, whereas for the other the Co atoms display in-plane antiferromagnetism. These results pave new avenues for designing two-dimensional (2D) metal-organic magnets and tailoring their inherent magnetic properties.

Introduction

The tendency toward miniaturization of technological devices has led to an increasing research interest on low-dimensional materials. Herein, the engineering of magnetic materials at the nanoscale could lead to the development of applications in the fields of spintronics or quantum computing.^[1,2] The early studies on magnetic nano-materials date from the late 1960's, with the report of transition-metal magnetic ultrathin films grown on metallic substrates.^[3,4] The research performed in this field resulted in the discovery of the giant magnetoresistance effect,^[5,6] leading to the beginning of spintronics.

The interest on the realization of truly two-dimensional (2D) magnets has been renewed by the discovery of van der

Waals heterostructures,^[7,8] materials composed of stacking layers with extended in-plane crystalline order and weak interlayer interaction. When the dimensionality of these materials is reduced to the 2D or quasi-2D limit, they frequently present electronic, optical and magnetic properties that diverge significantly from their bulk counterparts.^[9] Regarding magnetism, 2D van der Waals magnets can present either ferro or antiferromagnetic long-range ordering.^[2]

Besides these inorganic materials, low-dimensional magnetism can also be achieved in molecular compounds, as is the case of metal-organic frameworks (MOFs), which can exhibit intrinsic magnetism due to exchange interactions between the metallic centers. The exchange coupling can be reinforced using π -conjugated ligands, being seminal the work on 2D-layered MOFs, materials composed of stacking 2D layers

[*] S. K. Mathialagan⁺, Dr. S. O. Parreiras⁺, Dr. C. Martín-Fuentes, Dr. D. Moreno, L. Černa, Dr. M. Tenorio, Dr. B. Muñiz-Cano, Dr. K. Lauwaet, M. A. Valbuena, Dr. J. I. Urgel, Prof. R. Miranda, Prof. N. Martín, Prof. D. Écija

Institution Instituto Madrileño de Estudios Avanzados en Nanociencia (IMDEA Nanoscience), Madrid 28049, Spain

E-mail: sofia.oliveira@imdea.org nazmar@ucm.es

david.ecija@imdea.org

Dr. J. Santos⁺, Prof. N. Martín Departamento de Química Orgánica, Facultad de Química, Universidad Complutense, Madrid 28040, Spain

Dr. M. Tenorio, Dr. P. Gargiani Department of Materials, ETH Zürich, Zürich CH-8093, Switzerland Dr. M. Valvidares

ALBA Synchrotron Light Source, Barcelona 08290, Spain

Dr. J. I. Urgel, Prof. D. Écija

Unidad de Nanomateriales Avanzados, IMDEA Nanoscience, Unidad Asociada al CSIC por el ICMM, Madrid 28049, Spain

Prof W/ Kuch

Institut für Experimentalphysik, Freie Universität Berlin, Berlin 14195, Germany

Prof. R. Miranda

Departamento de Física de la Materia Condensada and Condensed Matter Physics Center (IFIMAC), Universidad Autónoma de Madrid, Madrid 28049, Spain

J. I. Martínez, Dr. J. M. Gallego

Instituto de Ciencia de Materiales de Madrid (ICMM), CSIC, Madrid 28049 Spain

E-mail: joseignacio.martinez@icmm.csic.es

- [+] These authors contributed equally to this work.
- Additional supporting information can be found online in the Supporting Information section





held together by intermolecular interactions.^[12] Some of these frameworks have been demonstrated to display magnetic ordering.^[13,14] However, it is worth mentioning that these materials are usually synthesized in wet chemistry and comprise multilayer stacks.

Coordination chemistry at surfaces has been proposed as an approach to grow one-atom thick 2D MOFs, also termed 2D metal-organic networks (2D MONs).[15] Onsurface synthesis allows the surface-confined growth of regular 2D arrays with long-range ordering, and has been extensively used for the preparation of metal-organic networks based on 3d or 4f metallic nodes coordinated with different molecular linkers.^[15–18] Regarding 2D metal-organic networks, a few systems have been reported to present magnetic ordering. An antiferromagnetic coupling was observed in Co-based networks with in-plane^[19] or out-of-plane^[20] magnetic anisotropy, while a very weak antiferromagnetic coupling was also observed for a Mn-based network.[21] Although a ferromagnetic coupling between metallic centers has previously been suggested, [21-23] magnetic hysteresis with non-zero remanence was explicitly observed only recently for an Fe-based network with an out-of-plane easy-axis.[24] Additionally, the reduced dimensionality due to the surface confinement has been proven to be an effective route to unquench the orbital magnetic moment, [20] which has led to an increased magnetic anisotropy.

Overall, coordination chemistry at interfaces has demonstrated great versatility to engineer 2D metal-organic networks with specific coordination environments. However, the study of the magnetic properties upon variation of their coordination environment, while keeping the same constituents, linkers and metal node, remains unexplored.

Here, we report the synthesis of two different 2D metal-organic nanoarchitectures based on the coordination of N,N'-dicyano-9,10-anthraquinonediimine^[25] (DCAQI, see Figure S1) linkers with cobalt (Co) atoms on a Au(111) surface. We investigated their structural, electronic, and magnetic properties by a comprehensive study comprising scanning tunneling microscopy (STM) and spectroscopy (STS), noncontact atomic force microscopy (nc-AFM), X-ray absorption spectroscopy (XAS), X-ray linear dichroism (XLD), and Xray magnetic circular dichroism (XMCD), complemented by first-principles density functional theory (DFT) atomistic calculations. Our results show that it is feasible to grow two different Co-based supramolecular 2D networks by regulating the cobalt-to-molecule stoichiometry ratio, thus making it possible to tailor the magnetic properties of the Co-directed nanoarchitectures by keeping the same molecular linker, while changing the coordination environment, thus modifying magnetic anisotropy and magnetization at 6 T applied magnetic field. This level of control over magnetic behavior is unprecedented, and highlights the power of surface-confined coordination chemistry at interfaces, where molecular-level modifications can lead to macroscopic changes in magnetic properties. Our studies open new avenues for the design and control of the magnetic properties of 2D metal-organic magnetic materials.

Results and Discussion

The deposition of DCAQI molecules (see Scheme 1) on a Au(111) surface gives rise to four different supramolecular self-assemblies (see Figure S2). Subsequent Co deposition on top of a submonolayer coverage of DCAQI on Au(111) and annealing in the range from 80 °C to 140 °C results in the formation of two distinct metal-organic phases regulated by the specific cobalt-to-molecule stoichiometric ratio (see Scheme 1 and Figure 1). The role of the annealing temperature is to control the domain size, since higher temperature promotes the growth of the average size of the domains (see Figure S3).

The first metal-organic nanoarchitecture, termed phase alpha and displayed in Figures 1a and \$5a,c, is a 2D supramolecular network. It is based on Co-directed metalorganic chains that rely on a two-fold Co-cyanimine coordination. Additional ligands are placed almost perpendicular to the chains, aligning them in a parallel fashion, presumably through weak two-fold Co-cyanimine interactions, which altogether result in a final oblique nanostructure. A constant height STM image of phase alpha is illustrated in Figure 1b, which evidences the electronic differences between the molecules forming the chains and the species aligning the wires. The molecules involved in the strong metal-organic coordination (linker motif 1) display a rounder shape with a bright center, while the weakly coordinated molecules (linker motif 2) have a more homogenous contrast, exhibiting three lobes assigned to the anthracene backbone of the linker. Our rationalization of the supramolecular assembly is ratified by non-contact AFM imaging using a CO-functionalized tip (Figure 1c), which allows to discern both, the molecular backbone and the cyanimine functional groups. An optimized DFT model of phase alpha is displayed in Figure 1d, based on a unit cell featuring an oblique lattice with lattice parameters of 13.3 Å and 18.2 Å. These values agree well with the experimental values of 13.8(4) Å and 17.5(6) Å. According to the DFT model the distance (see Figure 1f) between the N and Co atoms in the strong two-fold Co-cyanimine bond is 1.8 Å, whereas it is 4.4 Å for the weakly coordinated species, a difference in bond distance which is clearly appreciated in the nc-AFM image (see Figure 1e). Phase alpha presents rotational domains with different orientations with respect to the Au(111) substrate (see Figure S3).

The second metal-organic nanoarchitecture, termed phase beta and shown in Figures 1g and S5b,d, is a 2D Co-directed metal-organic network based on a three-fold Co-cyanimine coordination. The Co atoms are arranged in a honeycomb lattice, whereas the molecular species, with their anthracene moieties parallel to the Au(111) high symmetry directions, form a Kagome network. The optimized DFT model is presented in Figure 1h with the unit cell indicated by dashed lines. The size of the unit cell is 23.4 Å according to the theoretical calculations, and 23.8(4) Å based on experimental data. For phase beta the DFT calculations predict a N-Co bond distance of 2.0 Å (see Figure 1i). This phase is perfectly aligned to the high-symmetry directions of the Au(111) surface and forms monodomain islands (see Figure S4).

Research Article

Scheme 1. Conceptual scheme of the growth of Co-DCAQI nanoarchitectures on Au(111) affording phases alpha and beta by specific control of the cobalt-to-molecule stoichiometric ratio. Blue and red balls represent N and Co atoms, respectively.

The electronic properties of both metal-organic phases were inspected by STS (see Figure 2 for phase alpha and figure 3 for phase beta). Regarding phase alpha, a broad and strong resonance is observed above 1.8 eV (blue/grey dots and lines in Figure 2a,b) where the spatial distribution is over the rims of both the strongly and the weakly coordinated ligands (see Figure 2d). The STS measured at the Co atom shows a wide resonance at negative bias (\sim -0.8 V, red spectrum). Additionally, dI/dV maps taken at -50 mV and +50 mV are identical (see Figure 2e,f), revealing a state crossing zero bias, and, thus, experimentally pointing toward the metallic character of phase alpha. This finding is in excellent agreement with the associated DFT + U calculations, which predict that the system is metallic along the direction of the chains (see Figure S6). The spectrum measured at the Co atom features a dip at zero bias, which is better resolved by high-resolution STS (Figure 2c), whose plausible explanation is associated to the Kondo effect, since similar lineshapes were observed for Co impurities on a Au(111) surface. [26,27]

Concerning the electronic properties of phase beta, there is also a broad resonance around 1.8 eV (see Figure 3a,b) which is located at the rims of the linkers (see Figure 3d). Additionally, there is a dip for both the center of the linkers and the Co atoms, which are slightly off-centered from zero bias, as it can be observed in high-resolution STS (see Figure 3c). According to the DFT + U calculations (see Figure S7), there is an electronic band crossing the Fermi level. The absence of a band gap implies that this network is also metallic. Additionally, the projected density of states shows two peaks/features close to zero bias, one at negative binding energy and one at positive (Figure S7a). The latter one is positioned only slightly above zero bias and actually crosses it. This is very similar to the STS data, which shows two resonances, one at positive and the other one at negative biases, and the off-centered dip in between them for the cobalt center and the molecular linker. Also in this case, the positive resonance crosses zero bias. This resonance is attributed to the band crossing Fermi level predicted by the DFT calculations. Furthermore, dI/dV maps measured at low bias (65 and -177 meV, respectively) reveal the spatial distribution of the resonances measured by STS (Figure 3e,f).

DFT calculations were also performed to address the magnetism of the networks. Different spin configurations were explored, including non-magnetic, ferromagnetic and antiferromagnetic ground states. For the magnetic configurations, in-plane, out-of-plane and tilted spin orientations were considered. For phase alpha, the lower energy configuration is out-of-plane antiferromagnetic, and for phase beta, DFT predicts an in-plane antiferromagnetic ground state (see Figure S8).

Experimentally, the magnetic properties were investigated by XAS/XMCD/XLD measurements done at BOREAS beamline of the ALBA synchrotron light source.^[28] The experiments were performed at a nominal temperature of 2 K. Figure 4a,b presents background-subtracted XAS spectra measured with circularly polarized light and XMCD spectra taken at normal (0°, NI) and grazing (70°, GI) incidences. In the case of phase beta (Figure 4b), the XAS spectra present a fine multiplet structure that is characteristic of a + 2oxidation state.[19,29,30] The center of mass of the L₃ transition resonance is located around 778 eV, in agreement with a Co²⁺ state, whereas a Co3+ configuration results in a resonance above 780 eV.[19,29-32] For phase alpha (Figure 4a), the identification of the oxidation state is not so straightforward. The XAS spectra do not have the same fine multiplet structure; however, the energy of the peaks is the same as in the case of phase beta (around 778 eV). The XAS spectra measured with linearly polarized light (Figure 4c,d) present a comparable peak structure for the two networks, with more pronounced multiplet features in the phase beta. The XLD 15213773, 2023, 44, Downloaded from https://onlinelibtary.wiley.com/doi/10.1002/anie.20259199 by Freie Universitate Berlin, Wiley Online Libtary on [3]/10/2025]. See the Terms and Conditions (https://onlinelibtary.wiley.com/terms-and-conditions) on Wiley Online Libtary for rules of use; OA arcites are governed by the applicable Creative Commons Licensea

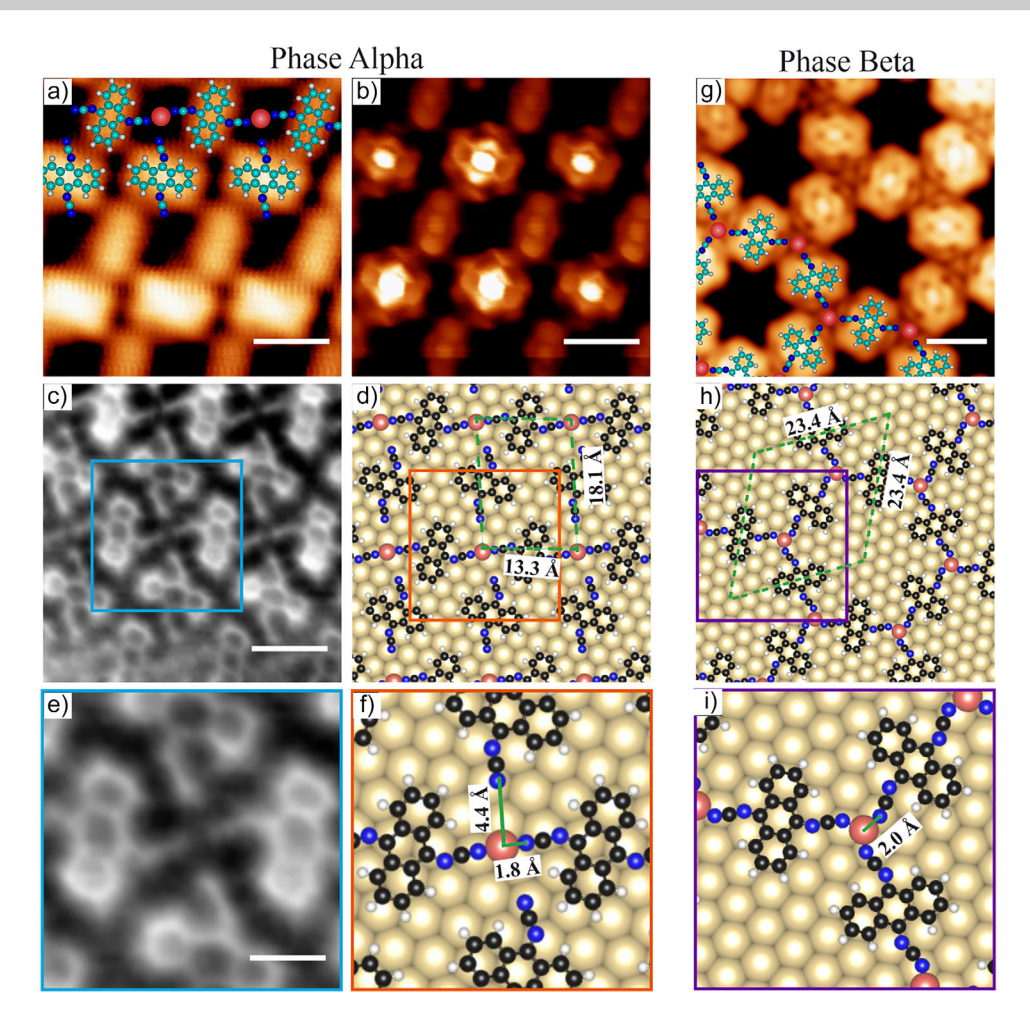


Figure 1. Structure of the two distinct Co-DCAQI nanoarchitectures on Au(111). a)–f) Phase alpha; g)–i) phase beta. a) High-resolution constant current STM image. b) High-resolution constant height STM image. c) non-contact AFM image. d) DFT optimized structure where Au, Co, C, N, and H atoms are depicted by yellow, red, black, blue and white spheres. The unit cell is represented by green dashed lines. e) Zoom-in of (c). f) Zoom-in of d), the N—Co bond distance is displayed by green lines. g) High-resolution constant current STM image. h) DFT optimized structure. The unit cell is represented by green dashed lines. i) Zoom-in of h), the N—Co bond distance is displayed by a green line. Scanning parameters: a) $I_t = 100$ pA, $V_{\text{bias}} = 500$ mV, T = 4.4 K, scale bar = 1 nm; b) open feedback: $I_t = 100$ pA, $V_{\text{bias}} = 5$ mV, $V_{\text{offset}} = 130$ pm, $V_{\text{bias}} = 5$ mV, $V_{\text{colset}} = 130$ pm, $V_{\text{bias}} = 100$ pA, $V_{\text{bias}} = 100$ p

spectra, obtained as the difference between linear vertical and linear horizontal XAS, present the same features in both phases indicating a similar electronic configuration of the Co ion. It is worth noting that the XLD features of phase alpha are less intense than their phase beta counterparts, suggesting that phase alpha is characterized by a more symmetric charge distribution or less intense ligand field around the Co atom compared to phase beta. Based on these evidences we assume that both phases present an oxidation state close to Co(II). Additionally, DFT calculations predict +1.09 and +1.21 oxidation states for phases alpha and beta, respectively, and considering that DFT underestimates the value of the oxidation states, such theoretical finding corroborates our assumption.

All XAS spectra measured for both phases present similar branching ratio $BR = L_3/(L_2 + L_3)$, with values ranging from 0.81 to 0.86. These values are much higher than the atomic branching ratio of 2/3, which points toward a high-spin state for both phases.

A comparison of the XMCD results for both phases reveals that phase alpha presents low intensity and almost isotropic magnetization. In contrast, phase beta shows a higher XMCD intensity, accompanied by in-plane magnetic anisotropy, as indicated by the stronger XMCD signal observed at GI compared to NI. Additionally, the XMCD magnetization curves highlight the differences in the magnetic behavior of the two phases (Figure 5). The curves measured for phase beta (Figure 5b) show a higher magnetization in the GI geometry, in agreement with the XMCD data at 6T, indicating the presence of magnetic anisotropy with inplane easy direction. For phase alpha the field dependent XMCD curves for GI and NI direction are nearly identical, indicating an isotropic magnetization. The low magnetization measured on both networks and the absence of magnetic remanence suggest a antiferromagnetic ordering of the Co ions.[19] These experimental results are thus consistent with DFT calculations, which predict out-of-plane and in-plane antiferromagnetism for phases alpha and beta, respectively. 15213773, 2025, 44, Downloaded from https://onlinelibrary.wiley.com/doi/10.1002/anie.20259199 by Free Universitate Berlin, Wiley Online Library on [31/10/2025]. See the Terms and Conditions (https://onlinelibrary.wiley.com/terms-mad-conditions) on Wiley Online Library for rules of use; OA articles are governed by the applicable Creative Commons. Licenses, and Conditions (https://onlinelibrary.wiley.com/terms-mad-conditions) on Wiley Online Library for rules of use; OA articles are governed by the applicable Creative Commons. Licenses, and Conditions (https://onlinelibrary.wiley.com/terms-mad-conditions) on Wiley Online Library for rules of use; OA articles are governed by the applicable Creative Commons. Licenses, and Conditions (https://onlinelibrary.wiley.com/terms-mad-conditions) on Wiley Online Library for rules of use; OA articles are governed by the applicable Creative Commons. Licenses, and Conditions (https://onlinelibrary.wiley.com/terms-mad-conditions) on Wiley Online Library for rules of use; OA articles are governed by the applicable Creative Commons. Licenses, and the conditions of the conditions o

Figure 2. Electronic properties of phase alpha of the Co-DCAQI nanoarchitecture on Au(111). a) Reference STM image for b) and c), indicating the positions where the spectra were taken. b), c) STS spectra measured at b) long range and c) short range close to zero bias. The spectra measured at Au(111), the Co atom, and the linker motifs 1 (strongly interacting molecules) and 2 (weakly interacting molecules) are represented by green, red, blue and grey lines, respectively. d), e), f) Topographic images and corresponding dI/dV maps at selected bias voltages. Scanning parameters: a) $I_t = 150$ pA, $V_{\text{bias}} = 2.0 \text{ V}$, T = 4.4 K, scale bar = 1 nm; d) $I_t = 400 \text{ pA}$, $V_{\text{bias}} = -50 \text{ mV}$, T = 4.4 K, scale bar = 1 nm; f) $I_t = 400 \text{ pA}$, $V_{\text{bias}} = 50 \text{ mV}$, T = 4.4 K, scale bar = 1 nm; f) $I_t = 400 \text{ pA}$, $V_{\text{bias}} = 50 \text{ mV}$, T = 4.4 K, scale bar = 1 nm; f) $I_t = 400 \text{ pA}$, $V_{\text{bias}} = 50 \text{ mV}$, $V_{\text{bias}} = 50 \text{ mV}$, $V_{\text{bias}} = 1 \text{ nm}$; f) $V_t = 4.4 \text{ K}$, scale bar = 1 nm; f) $V_t = 4.4 \text{ K}$

Herein, the weaker XMCD signal for phase alpha could be attributed to a stronger antiferromagnetic exchange coupling compared to phase beta.

The expectation values of the magnetic moments calculated by applying the sum rules^[34,35] to the experimental spectra measured at 6 T are shown in Table 1. Phase alpha presents similar moments at both incidences, with differences within the experimental error. The effective spin moment is 0.25(3) h. Phase beta has a higher magnetic moment at GI, reflecting an in-plane anisotropy. However, the orbital-to-effective-spin ratio is larger for phase alpha, indicating that the different coordination changes the degree of quenching of the orbital magnetic moment. For phase beta the experimental effective spin moment at GI is 0.69(7) h.

As discussed previously, the branching ratio of L_2 and L_3 peaks is the same for both phases, and its high value suggests a high-spin state. It should be noted that the magnetic moments calculated by sum rules represent expectation values of the moments projected along the beam incidence direction at the experimental conditions of 2 K and 6 T, and they should be considered as lower limits for the real magnetic moments, since, as can be observed in Figure 5, none of the systems is at saturation at these conditions. In this situation the branching ratio is a better indication of the spin state. Considering that the experimental results are compatible with S=3/2 for

both systems. The DFT calculations predict a total spin of 1.46 per Co atom for phase alpha and 1.04 for phase beta. However, the DFT values account for s and d electrons, while the XMCD of $L_{2,3}$ edges measures only the moment from d electrons. When only d electrons are taken into account, the theoretical spin is 1.43 for phase alpha and 1.46 for phase beta, in agreement with S=3/2 for both phases.

Conclusion

We report the design of two-dimensional metal-organic nanoarchitectures driven by the coordination of DCAQI linkers with Co atoms on a Au(111) surface. Two different phases with long-range ordering are formed depending on the stoichiometry. Both phases are metallic, present an oxidation state close to Co(II), but show very distinct magnetic properties. The experimental results together with the DFT calculations point toward out-of-plane antiferromagnetism with S=3/2 for phase alpha, while the findings for phase beta are consistent with weak in-plane antiferromagnetism and S=3/2. Our results demonstrate that coordination chemistry can tailor the inherent magnetic properties of metal-organic nanoarchitectures by customizing the coordination sphere, thereby opening avenues for the design of two-dimensional molecular magnetic materials.



15217373, 2025, 44, Downloaded from https://onlineliblary.wiley.com/oi/10.1002/anie.202509199 by Free Universitated Berlin, Wiley Online Library on [31/10/2025]. See the Terms and Conditions (https://onlinelibrary.wiley.com/terms-and-conditions) on Wiley Online Library or rules of use; OA articles are governed by the applicable Creative Commons License

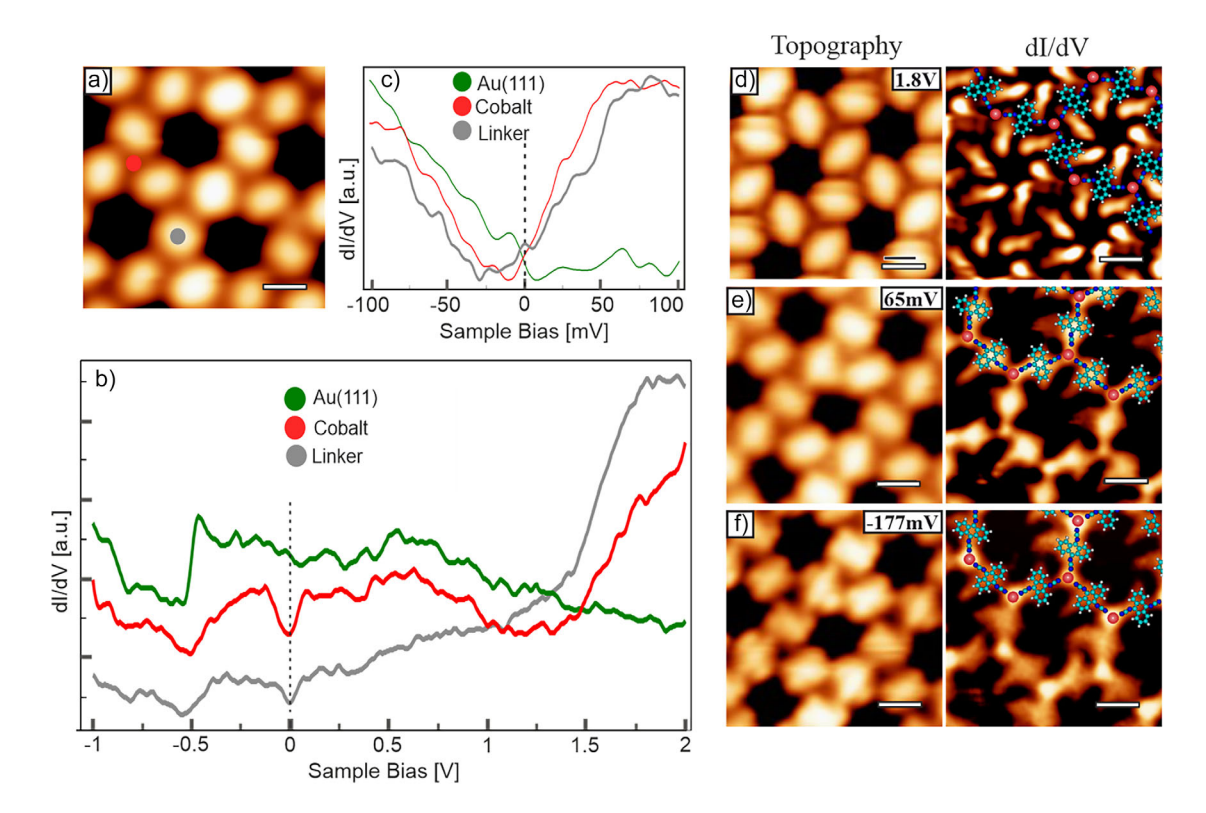


Figure 3. Electronic properties of phase beta of the Co-DCAQI nanoarchitecture on Au(111). a) Reference STM image for b) and c), indicating the positions where the spectra were taken. b), c) STS spectra measured at b) long range and c) short range close to zero bias. The spectra measured at Au(111), Co atom and the molecular linker are represented by green, red and grey lines, respectively. d), e), f) Topographi images and corresponding dI/dV maps at selected bias voltages. Scanning parameters: a) $I_t = 20$ pA, $V_{\text{bias}} = 500$ mV, T = 4 K, scale bar = 1 nm; d) $I_t = 400$ pA, $V_{\text{bias}} = 1.8$ V, T = 4 K, scale bar = 1 nm; e) $I_t = 200$ pA, $V_{\text{bias}} = 65$ mV, T = 4 K, scale bar = 1 nm; f) $I_t = 200$ pA, $V_{\text{bias}} = -177$ mV, T = 4 K, scale bar = 1 nm.

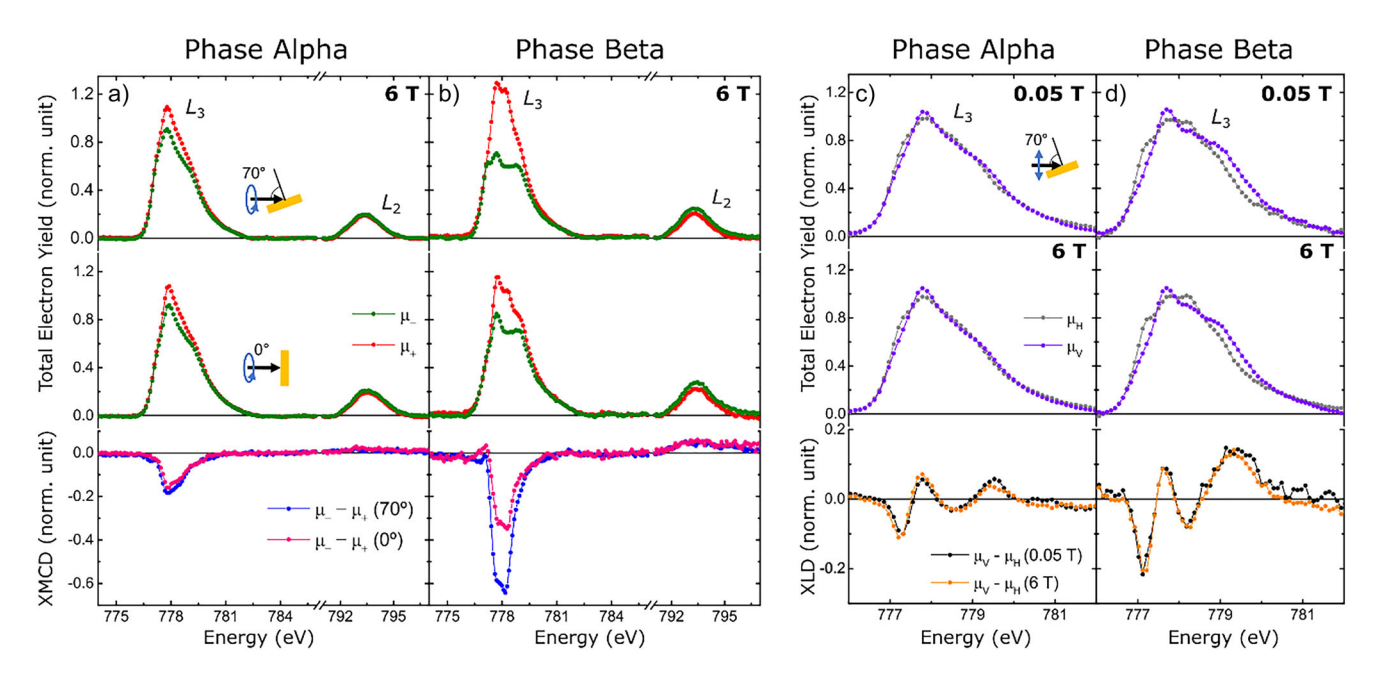


Figure 4. XAS spectra of the Co-DCAQI nanoarchitectures on Au(111). a)–b) XAS spectra with negative (μ_- , green) and positive (μ_+ , red) circularly polarized light and XMCD ($\mu_- - \mu_+$) taken at the Co $L_{2,3}$ edges at normal (0°, pink) and grazing (70°, blue) incidences for the phases a) alpha and b) beta (B=6 T). c)–d) XAS spectra acquired with horizontal (μ_H , gray) and vertical (μ_V , purple) linearly polarized light and XLD ($\mu_V - \mu_H$) taken at Co L_3 -edge at grazing incidence for fields of 0.05 T (black) and 6 T (orange) for the phases c) alpha and d) beta.

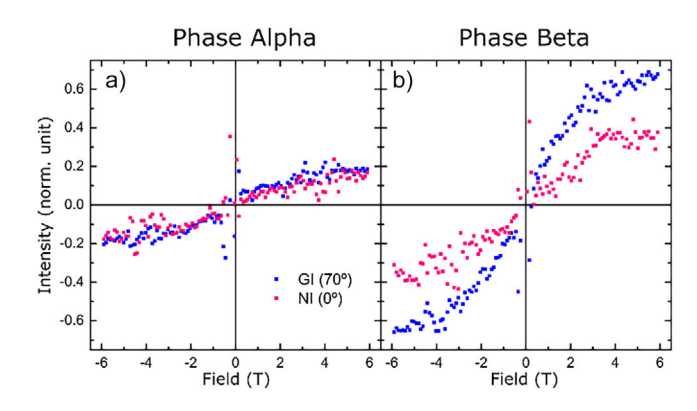


Figure 5. Magnetization curves of the Co-DCAQI nanoarchitectures on Au(111). Magnetization curves of the phases a) alpha and b) beta acquired by measuring the XMCD intensity at the most intense peak of the Co L_3 -edge at normal (0°, pink) and grazing (70°, blue) incidences, normalized to the respective helicity-averaged L_3 peak height.

Table 1: Effective spin ($\langle S_{eff} \rangle$) and orbital ($\langle L_z \rangle$) operators in \hbar units, orbital-to-effective-spin moment ratio ($\langle L_z \rangle/2 \langle S_{eff} \rangle$), effective spin ($m_{S_{eff}}$), orbital (m_L) and total ($m_T = m_L + m_{S_{eff}}$) magnetic moments in μ_B , extracted by XMCD sum rules for normal (0°) and grazing (70°) incidences at 6 T for Co centers on Co-DCAQI networks on Au(111).

Phase	Alpha		Beta	
Incidence angle (°)	70	0	70	0
$\langle S_{eff} \rangle$ (ħ)	0.25(3)	0.24(2)	0.69(7)	0.43(4)
$\langle L_z \rangle$ (ħ)	0.21(2)	0.23(2)	0.52(5)	0.26(3)
$\langle L_z \rangle / 2 \langle S_{eff} \rangle$	0.42(6)	0.48(6)	0.38(5)	0.29(4)
$m_{S_{eff}}$ (μ_{B})	0.49(6)	0.48(4)	1.38 (14)	0.86(8)
$m_L (\mu_B)$	0.21(2)	0.23(2)	0.52(5)	0.26(3)
m_T (μ_B)	0.70(8)	0.71(6)	1.90(19)	1.12(11)

Supporting Information

The authors have cited additional references within the Supporting Information.^[36–52]

Acknowledgements

The authors acknowledge the funding from the Spanish MICINN and the Spanish Research Agency MICIN/AEI PID2023-146373OB-I00, PID2022-136961NB-PID2021-123776NB-C21, PID2023-149077OB-C31, PLEC2021-007906, RED2022-134503-T, PDC2023-145871-I00 and TED2021-129416A-I00), and from Comunidad Autónoma de Madrid via "Programa de Investigación Tecnologías" 2020 (FOTOSURF-CM Y2020/NMT-6469) and 2024 (SYNMOLMAT-CM TEC-2024/TEC-459), cofinanced by European Structural Funds. The authors thank support from the "(MAD2D-CM)-IMDEA-Nanociencia" and "(MAD2D-CM)-UCM" projects funded by Comunidad de Madrid, by the Recovery, Transformation and Resilience Plan, and by NextGenerationEU from the European Union. The authors also acknowledge the funding from PERTE Chip project PDC2023-145871-I00. N.M. and J.S. acknowledge financial support from the ERC (SyG TOMATTO ERC-2020-951224). IMDEA Nanociencia acknowledges financial support from the ERC (CoG ELECNANO ERC-2018-766555) and the Spanish Ministry of Science and Innovation "Severo Ochoa" (Grant CEX2020-001039-S). ALBA synchrotron is acknowledged for providing beamtime (proposal numbers 2022097056 and 2021025046).

Conflict of Interests

The authors declare no conflict of interest.

Data Availability Statement

The data that support the findings of this study are openly available in https://repositorio.imdeananociencia.org.

Keywords: Coordination chemistry • Density functional theory • Magnetic anisotropy • Scanning tunneling microscopy • X-ray magnetic circular dichroism

- D. L. Cortie, G. L. Causer, K. C. Rule, H. Fritzsche, W. Kreuzpaintner, F. Klose, Adv. Funct. Mater. 2020, 30, 1901414.
- [2] C. Gong, X. Zhang, Science 2019, 363, 706.
- [3] U. Gradmann, Ann. Phys. 1966, 472, 91-106.
- [4] U. Gradmann, J. Müller, J. Appl. Phys. 1968, 39, 1379–1381.
- [5] G. Binasch, P. Grünberg, F. Saurenbach, W. Zinn, Phys. Rev. B 1989, 39, 4828–4830.
- [6] M. N. Baibich, J. M. Broto, A. Fert, F. Nguyen Van Dau, F. Petroff, P. Etienne, G. Creuzet, A. Friederich, J. Chazelas, *Phys. Rev. Lett.* 1988, 61, 2472–2475.
- [7] B. Huang, G. Clark, E. Navarro-Moratalla, D. R. Klein, R. Cheng, K. L. Seyler, D. Zhong, E. Schmidgall, M. A. McGuire, D. H. Cobden, W. Yao, D. Xiao, P. Jarillo-Herrero, X.-D. Xu, *Nature* 2017, 546, 270–273.
- [8] C. Gong, L. Li, Z. Li, H. Ji, A. Stern, Y. Xia, T. Cao, W. Bao, C. Wang, Y. Wang, Z. Q. Qiu, R. J. Cava, S. G. Louie, J. Xia, X. Zhang, *Nature* 2017, 546, 265–269.
- [9] P. Ajayan, P. Kim, K. Banerjee, Phys. Today 2016, 69, 38-44.
- [10] A. E. Thorarinsdottir, T. D. Harris, Chem. Rev. 2020, 120, 8716– 8789.
- [11] X. Yan, X. Su, J. Chen, C. Jin, L. Chen, Angew. Chem. Int. Ed. 2023, 62, e202305408.
- [12] L. S. Xie, G. Skorupskii, M. Dincă, Chem. Rev. 2020, 120, 8536– 8580.
- [13] C. Yang, R. Dong, M. Wang, P. St Petkov, Z. Zhang, M. Wang, P. Han, M. Ballabio, S. A. Bräuninger, Z. Liao, J. Zhang, F. Schwotzer, E. Zschech, H.-H. Klauss, E. Cánovas, S. Kaskel, M. Bonn, S. Zhou, T. Heine, X. Feng, *Nat. Commun.* 2019, 10, 3260.
- [14] R. Dong, Z. Zhang, D. C. Tranca, S. Zhou, M. Wang, P. Adler, Z. Liao, F. Liu, Y. Sun, W. Shi, Z. Zhang, E. Zschech, S. C. B. Mannsfeld, C. Felser, X. Feng, *Nat. Commun.* 2018, 9, 2637.
- [15] J. Liu, M. Abel, N. Lin, J. Phys. Chem. Lett. 2022, 13, 1356–1365.
- [16] J. V. Barth, Annu. Rev. Phys. Chem. 2007, 58, 375.
- [17] L. Dong, Z. Gao, N. Lin, Prog. Surf. Sci. 2016, 91, 101–135.
- [18] S. O. Parreiras, J. M. Gallego, D. Écija, Chem. Commun. 2023, 59, 8878–8893.
- [19] C. Martín-Fuentes, S. O. Parreiras, J. I. Urgel, V. Rubio-Giménez, B. M. Cano, D. Moreno, K. Lauwaet, M. Valvidares, M. A. Valbuena, P. Gargiani, W. Kuch, J. Camarero, J. M. Gallego, R. Miranda, J. I. Martínez, C. Martí-Gastaldo, D. Écija, J. Am. Chem. Soc. 2022, 144, 16034–16041.

15213773, 2025, 44, Downloaded from https://onlinelibrary.wiley.com/dbi/10.1002/anie.202509199 by Free Universitatet Berlin, Wiley Online Library on [31/10/2025], See the Terms and Conditions (https://onlinelibrary.wiley.com/terms-and-conditions) on Wiley Online Library for rules of use; OA articles are governed by the applicable Creative Commons Licenses

Research Article



15213773, 2025, 44, Downloaded from https://onlinelibrary.wiley.com/doi/10.1002/anie.202509199 by Freie Universitaet Berlin, Wiley Online Library on [31/10/2025]. See the Terms and Conditions (https://onlinelibrary.wiley.com/ems/

and-conditions) on Wiley Online Library for rules of use; OA articles are governed by the applicable Creative Commons License

- [20] S. O. Parreiras, C. Martín-Fuentes, D. Moreno, S. K. Mathialagan, K. Biswas, B. Muñiz-Cano, K. Lauwaet, M. Valvidares, M. A. Valbuena, J. I. Urgel, P. Gargiani, J. Camarero, R. Miranda, J. I. Martínez, J. M. Gallego, D. Écija, Small 2024, 20, 2309555.
- [21] M. N. Faraggi, V. N. Golovach, S. Stepanow, T.-C. Tseng, N. Abdurakhmanova, C. S. Kley, A. Langner, V. Sessi, K. Kern, A. Arnau, J. Phys. Chem. C 2015, 119, 547–555.
- [22] T. R. Umbach, M. Bernien, C. F. Hermanns, A. Krüger, V. Sessi, I. Fernandez-Torrente, P. Stoll, J. I. Pascual, K. J. Franke, W. Kuch, Phys. Rev. Lett. 2012, 109, 267207.
- [23] L. Giovanelli, A. Savoyant, M. Abel, F. Maccherozzi, Y. Ksari, M. Koudia, R. Hayn, F. Choueikani, E. Otero, P. Ohresser, J.-M. Themlin, S. S. Dhesi, S. Clair, J. Phys. Chem. C 2014, 118, 11738–11744.
- [24] J. Lobo-Checa, L. Hernández-López, M. M. Otrokov, I. Piquero-Zulaica, A. E. Candia, P. Gargiani, D. Serrate, F. Delgado, M. Valvidares, J. Cerdá, A. Arnau, F. Bartolomé, *Nat. Commun.* 2024, 15, 1858.
- [25] A. Aumüller, S. Hünig, *Liebigs Ann. Chem.* **1985**, 142–164.
- [26] V. Madhavan, W. Chen, T. Jamneala, M. F. Crommie, N. S. Wingreen, *Science* 1998, 280, 567–569.
- [27] V. Madhavan, W. Chen, T. Jamneala, M. F. Crommie, *Phys. Rev. B* 2001, 64, 165412.
- [28] A. Barla, J. Nicolas, D. Cocco, S. M. Valvidares, J. Herrero-Martín, P. Gargiani, J. Moldes, C. Ruget, E. Pellegrin, S. Ferrer, J. Synchrotron Radiat. 2016, 23, 1507–1517.
- [29] A. Mandziak, D. G. Soria, J. E. Prieto, P. Prieto, C. Granados-Miralles, A. Quesada, M. Foerster, L. Aballe, J. de la Figuera, Sci. Rep. 2019, 9, 13584.
- [30] V. R. Singh, Y. Sakamoto, T. Kataoka, M. Kobayashi, Y. Yamazaki, A. Fujimori, F.-H. Chang, D.-J. Huang, H.-J. Lin, C. T. Chen, H. Toyosaki, T. Fukumura, M. Kawasaki, J. Phys.: Condens. Matter. 2011, 23, 176001.
- [31] Z. Hu, H. Wu, M. W. Haverkort, H. H. Hsieh, H.-J. Lin, T. Lorenz, J. Baier, A. Reichl, I. Bonn, C. Felser, A. Tanaka, C. T. Chen, L. H. Tjeng, *Phys. Rev. Lett.* 2004, 92, 207402.
- [32] N. Hollmann, Z. Hu, M. Valldor, A. Maignan, A. Tanaka, H. H. Hsieh, H.-J. Lin, C. T. Chen, L. H. Tjeng, *Phys. Rev. B.* 2009, 80, 085111.
- [33] B. T. Thole, G. van der Laan, Phys. Rev. B. 1988, 38, 3158-3171.
- [34] B. T. Thole, P. Carra, F. Sette, G.v. d. Laan, Phys. Rev. Lett. 1992, 68, 1943–1946.
- [35] P. Carra, B. T. Thole, M. Altarelli, X. Wang, Phys. Rev. Lett. 1993, 70, 694–697.
- [36] L. Bartels, G. Meyer, K.-H. Rieder, D. Velic, E. Knoesel, A. Hotzel, M. Wolf, G. Ertl, *Phys. Rev. Lett.* **1998**, 80, 2004–2007.

- [37] L. Gross, F. Mohn, N. Moll, P. Liljeroth, G. Meyer, Science 2009, 325, 1110–1114.
- [38] I. Horcas, R. Fernández, J. M. Gómez-Rodríguez, J. Colchero, J. Gómez-Herrero, A. M. Baro, Rev. Sci. Instrum. 2007, 78, 013705.
- [39] M. J. Frisch, G. W. Trucks, H. B. Schlegel, G. E. Scuseria, M. A. Robb, J. R. Cheeseman, G. Scalmani, V. Barone, G. A. Petersson, H. Nakatsuji, X. Li, M. Caricato, A. V. Marenich, J. Bloino, B. G. Janesko, R. Gomperts, B. Mennucci, H. P. Hratchian, J. V. Ortiz, A. F. Izmaylov, J. L. Sonnenberg, D. Williams-Young, F. Ding, F. Lipparini, F. Egidi, J. Goings, B. Peng, A. Petrone, T. Henderson, D. Ranasinghe, et al, Gaussian 16, Revision C.01, Gaussian, Inc., Wallingford CT, 2016
- [40] P. Giannozzi, S. Baroni, N. Bonini, M. Calandra, R. Car, C. Cavazzoni, D. Ceresoli, G. L. Chiarotti, M. Cococcioni, I. Dabo, A. Dal Corso, S. de Gironcoli, S. Fabris, G. Fratesi, R. Gebauer, U. Gerstmann, C. Gougoussis, A. Kokalj, M. Lazzeri, L. Martin-Samos, N. Marzari, F. Mauri, R. Mazzarello, S. Paolini, A. Pasquarello, L. Paulatto, C. Sbraccia, S. Scandolo, G. Sclauzero, A. P. Seitsonen, et al, J. Phys.: Condens. Matter 2009, 21, 395502.
- [41] A. D. Becke, J. Chem. Phys. 1993, 98, 5648-5652.
- [42] T. H. Dunning, J. Chem. Phys. 1989, 90, 1007-1023.
- [43] J. P. Perdew, A. Ruzsinszky, G. I. Csonka, O. A. Vydrov, G. E. Scuseria, L. A. Constantin, X. Zhou, K. Burke, *Phys. Rev. Lett.* 2008, 100, 136406.
- [44] G. Kresse, J. Joubert, Phys. Rev. B 1999, 59, 1758-1775.
- [45] S. Grimme, J. Comput. Chem. 2006, 27, 1787–1799.
- [46] H. J. Monkhorst, J. D. Pack, Phys. Rev. B 1976, 13, 5188–5192.
- [47] J. Hubbard, Proc. R. Soc. London A 1963, 276, 238-257.
- [48] J. Hubbard, Proc. R. Soc. London A 1967, 296, 100-112.
- [49] M. Capdevila-Cortada, Z. Łodziana, N. López, ACS Catal. 2016, 6, 8370–8379.
- [50] J. P. Lewis, P. Jelínek, J. Ortega, A. A. Demkov, D. G. Trabada, B. Haycock, G. Adams, J. K. Tomfohr, E. Abad, H. Wang, D. A. Drabold, *Phys. Status Solidi B* 2011, 248, 1989–2007.
- [51] A. A. Demkov, J. Ortega, O. F. Sankey, M. P. Grumbach, Phys. Rev. B: Condens. Matter Mater. Phys. 1995, 52, 1618– 1620
- [52] E. Ruiz, S. Alvarez, J. Cano, V. Polo, J. Chem. Phys. 2005, 123, 074102.

Manuscript received: April 25, 2025 Revised manuscript received: July 11, 2025 Manuscript accepted: August 20, 2025 Version of record online: September 10, 2025